Computers in Earth Science Letters (2026) 01-07

Contents lists available at FoundAE

Computers in Earth Science Letters

Journal homepage: https://ejournal.foundae.com/index.php/cesl/index

Delineation of shallow fault structures along the Sianok segment of the Sumatra fault using dipole–dipole electrical resistivity imaging

Gabriella A Sihite[a,*,1], Alamta Singarimbun[b,1], Marjiyono[c], Ahmad Said[d]

[a] Department of Physics, Institut Teknologi Sumatera, Way Huwi, Jati Agung, South Lampung, Lampung 35365, Indonesia
[b] Department of Physics, Faculty of Mathematics and Natural Sciences, Institut Teknologi Bandung, East Java 40132, Indonesia
[c] Centre for Geological Survey, Energy and Mineral Resources Ministry, Cibeunying Kaler, Bandung, East Java 40122, Indonesia
[d] Friedrich-Schiller-University Jena, Friedrich-Schellingstr, 07745 Jena, Germany

ARTICLE INFO

Keywords:
Sumatra Fault
Sianok segment
ERT
Dipole–dipole
Fault damage zone
Hazard assessment

ABSTRACT

The Sianok segment of the Sumatra Fault is an active tectonic structure that plays a critical role in controlling seismic hazards in West Sumatra, Indonesia. Despite its significance, detailed information on the shallow subsurface characteristics of this fault segment remains limited, particularly regarding the spatial variability of fault-related deformation near the surface. This study applies high-resolution two-dimensional electrical resistivity tomography (ERT) using a dipole–dipole configuration to delineate shallow fault structures along the Sianok segment. Seven ERT profiles were acquired across locations selected based on lineament interpretation from Digital Elevation Model (DEM) data that intersect the mapped trace of the Sumatra Fault. The resistivity data were inverted using a smoothness constrained least-squares algorithm implemented in Res2Dinv to generate two-dimensional subsurface resistivity models. The resulting sections reveal pronounced lateral resistivity contrasts, disrupted stratigraphic patterns, and localized resistivity anomalies interpreted as fault-related deformation zones. The identified fault zones exhibit a wide range of resistivity values, from approximately 7.6 to 29,684 Ωm, reflecting variations in lithology including clay, sand, alluvium, tuffaceous sandstone, sandstone, and volcanic tuff. Interpretation of the resistivity sections indicates the presence of both steeply dipping and westward-inclined fault geometries across different profiles. Several lines display resistivity patterns consistent with vertical displacement associated with normal faulting, while others show features indicative of strike-slip–related deformation. The spatial correspondence between subsurface resistivity anomalies and DEM-derived lineaments provides independent validation of the surface expression of the Sianok segment and confirms the presence of shallow fault structures along all investigated profiles. This study demonstrates that dipole–dipole ERT, when guided by geomorphological lineament analysis, is an effective method for resolving shallow fault architecture in complex volcanic–sedimentary terrains. The results provide new quantitative constraints on the shallow subsurface expression of the Sianok segment of the Sumatra Fault, contributing to improved fault characterization and regional seismic hazard assessment.

1. Introduction

Active strike-slip faults represent major sources of seismic hazard in tectonically active regions, particularly where fault systems traverse densely populated areas. Understanding the shallow subsurface characteristics of such faults is essential, as near-surface fault geometry and deformation zones strongly influence earthquake rupture propagation, ground shaking amplification, and surface deformation patterns [1, 2]. However, direct observations of fault structures are often limited to surface expressions, while the shallow subsurface architecture remains poorly constrained.

The Sumatra Fault is one of the most prominent active strike-slip fault systems in Southeast Asia, extending for more than 1,900 km along the backbone of Sumatra Island as a response to oblique convergence between the Indo-Australian and Eurasian plates [3–5]. This fault system is segmented (Fig. 1), with each segment exhibiting distinct geometrical and kinematic characteristics that influence its seismic behavior [6, 7]. Among these, the Sianok segment in West Sumatra is recognized as an active segment that has generated damaging earthquakes and poses a significant seismic risk to surrounding communities [8–10].

* Corresponding author.
E-mail address: gabriellasihite26@gmail.com (G. A. Sihite).
[1] These authors contributed equally to this work.

https://doi.org/10.58524/cesl.v1i1.100
Received 1 January 2026; Received in revised form 1 February 2026; Accepted 10 February 2026
Available online 1 March 2026
XXXX-XXXX/Published by FoundAE (Foundation of Advanced Education).

Previous investigations of the Sumatra Fault have primarily relied on geomorphological mapping, trenching studies, and regional seismological analyses to delineate fault traces and assess slip behavior [3, 11]. While these approaches provide valuable insights into surface deformation and long-term fault activity, they offer limited resolution of shallow subsurface fault structures, particularly in areas covered by thick sediments or volcanic deposits. In such settings, geophysical methods become essential for imaging subsurface fault zones and deformation patterns [12, 13].

Electrical resistivity tomography (ERT) has been widely applied to fault investigations due to its sensitivity to lithological contrasts, fracture density, and fluid content, all of which are key characteristics of fault damage zones [6, 14, 15]. In particular, the dipole–dipole configuration provides high lateral resolution and is well suited for imaging near-vertical structures such as strike-slip faults [4, 16]. When combined with geomorphological lineament analysis derived from Digital Elevation Model (DEM) data, ERT surveys can be strategically positioned to maximize their effectiveness in resolving shallow fault architecture [17, 18].

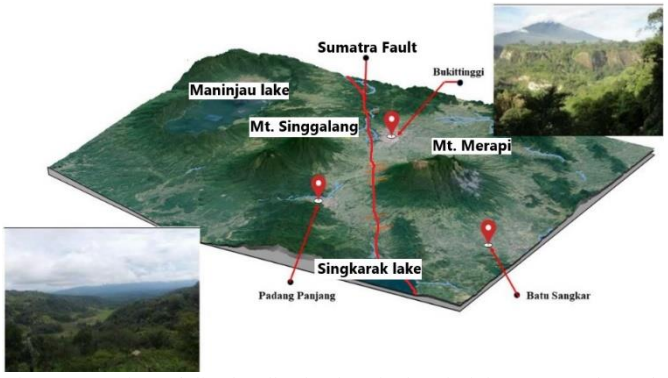

Fig. 1. Location of dipole–dipole electrical resistivity survey along the Sianok fault segment with geology information.

Geologically, the Sianok segment traverses a complex volcanic–sedimentary environment composed of Quaternary alluvial deposits, volcanic tuffs, tuffaceous sandstones, and older sedimentary units associated with the Bukit Barisan volcanic arc [3, 6, 16]. This heterogeneous geological setting produces strong lateral and vertical variations in electrical resistivity, offering favorable conditions for fault detection using ERT while simultaneously increasing the complexity of subsurface interpretation [19–21].

In this study, we apply high-resolution two-dimensional electrical resistivity tomography using a dipole–dipole configuration along seven profiles crossing DEM-derived lineaments associated with the Sianok segment of the Sumatra Fault. The objectives of this study are to (1) delineate shallow fault-related structures based on resistivity contrasts and deformation patterns, (2) characterize the spatial variability of shallow fault geometry along the segment, and (3) validate surface lineament interpretations with subsurface geophysical evidence. By providing quantitative constraints on the shallow subsurface expression of the Sianok segment, this work contributes to improved fault characterization and supports ongoing efforts in seismic hazard assessment in West Sumatra, Indonesia.

2. Method

2.1. Study area and data source

This study focuses on the Sianok segment of the Sumatra Fault located in Agam and Tanah Datar regencies, West Sumatra, Indonesia. Geographically, the study area extends between 100°19′29.0″E–100°31′49.0″E and 0°16′7.2″S–0°32′46.7″S (Fig. 2). The Sianok segment is geomorphologically expressed by linear valleys, fault-controlled escarpments, and aligned drainage systems associated with active tectonic deformation.

The research was conducted between January and April 2023 at Institut Teknologi Sumatera. Electrical resistivity data used in this study are secondary datasets acquired in 2015 by the Geological Survey Center, Ministry of Energy and Mineral Resources of Indonesia. The dataset consists of dipole–dipole electrical resistivity measurements stored in .dat format and includes apparent resistivity values, electrode spacing, measurement geometry, and topographic information.

Seven electrical resistivity profiles (ATG, BPL, BKM, KBA, SWU, BTP, and TGK) were selected to cross the interpreted trace of the Sumatra Fault. Profile locations and lengths range from 110 to 275 m and were determined to intersect fault-related lineaments identified from Digital Elevation Model (DEM) analysis. Detailed coordinates and profile descriptions are summarized in Table 1.

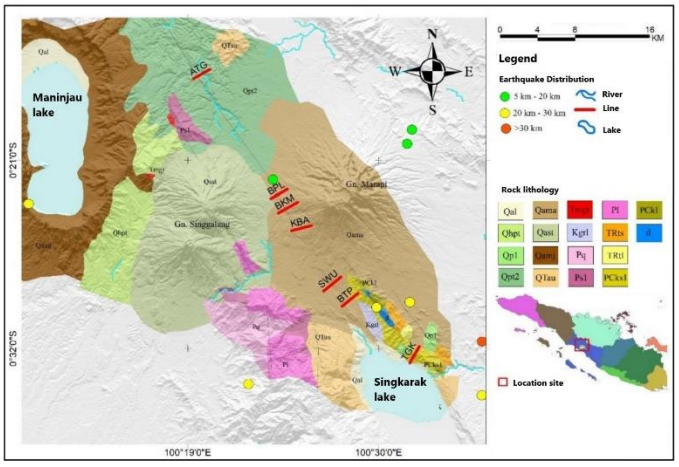

Fig. 2. Location of dipole–dipole electrical resistivity survey along the Sianok fault segment with geology information.

Table 1
Locations of electrical resistivity survey lines

No	Survey line	Longitude (E)	Latitude (S)	Line length	Location description
1	ATG	100°19′29.0″	0°16′7.2″	220 m	Jorong Aia Taganang, Tanjung Raya District, Agam Regency
2	BPL	100°23′58.6″	0°23′7.0″	110 m	Jorong Padang Giring-giring, Batu Palano, Sungai Puar District, Agam Regency
3	BKM	100°24′24.5″	0°23′56.6″	110 m	In front of Bika Mariana (Koto Baru), Aie Angek Village, X Koto District, Tanah Datar Regency
4	KBA	100°25′2.64″	0°25′4.04″	275 m	Jorong Kubu Diateh, Panyalaian Village, X Koto District, Tanah Datar Regency
5	SWU	100°27′17.6″	0°28′11.6″	110 m	Rice field area at the edge of Batipuh
6	BTP	100°28′5.1″	0°29′20.8″	165 m	MTsN Pitalah, Pitalah Road, Batipuh District, Tanah Datar Regency
7	TGK	100°31′49.0″	0°32′46.7″	165 m	Nagari III Koto

2.2. Electrical resistivity survey configuration

Electrical resistivity tomography (ERT) was conducted using a dipole–dipole electrode configuration. This array was selected due to its high sensitivity to lateral resistivity variations and its effectiveness in imaging steeply dipping and near-vertical structures commonly associated with strike-slip and oblique fault systems. The dipole–dipole configuration also provides improved lateral resolution compared to other common arrays, making it suitable for delineating fault-related deformation zones in shallow subsurface environments [14, 22, 23].

Each survey line consisted of evenly spaced electrodes deployed along a straight profile oriented approximately perpendicular to the regional fault strike. Apparent resistivity measurements were obtained by systematically increasing the dipole separation factor (n) to achieve greater depth of investigation while maintaining acceptable signal quality.

2.3. Electrical resistivity data processing and model analysis

Apparent resistivity data were processed and inverted using the RES2DINV software package. A smoothness-constrained least-squares inversion algorithm was applied to obtain two-dimensional subsurface resistivity models for each survey line. During the inversion process, iterative calculations were performed until the root mean square (RMS) error was reduced to less than 5%, ensuring a reliable fit between observed and calculated data. Noisy or anomalous data points associated with poor electrode contact or measurement errors were removed to improve inversion stability. Topographic corrections were incorporated into the inversion using elevation data collected along each profile.

The resulting two-dimensional resistivity sections were analyzed to identify subsurface lithological variations and structural discontinuities. Resistivity contrasts were interpreted based on established resistivity ranges, geological maps, and previous studies in the region.

High-resistivity zones were interpreted as compact and relatively dry rock units, whereas low-resistivity zones were associated with weathered materials, clay-rich layers, or water-saturated fractured zones. Abrupt lateral changes in resistivity and vertically continuous low-resistivity features were interpreted as shallow fault zones or fracture corridors.

Fault structures were identified based on sudden resistivity discontinuities, vertically aligned low-resistivity anomalies, and consistent structural patterns across multiple survey lines. These geophysical interpretations were validated by correlating resistivity models with regional geological maps, DEM-derived lineaments, and previous geological and seismotectonic studies. Visualization and comparative interpretation of resistivity sections were supported using Surfer software, facilitating clearer representation of lithological boundaries and fault geometries.

3. Results and discussion

3.1. Lithological identification and fault occurrence

Electrical resistivity imaging surveys were conducted in Agam and Tanah Datar Regencies using a dipole–dipole electrode configuration, which provides enhanced sensitivity to lateral resistivity variations and is particularly effective for detecting near-vertical structures such as faults. The acquired datasets were processed using RES2DINV, and the resulting two-dimensional resistivity sections were analyzed to delineate subsurface lithology and identify fault-related features, taking into account the regional geological framework.

Based on regional geological maps and previous studies (Table 2), the study area is composed of a wide range of lithological units, spanning from Quaternary to Permian–Carboniferous ages. The youngest units consist of Holocene alluvial deposits (Qal) composed of sand, silt, gravel, and reworked pumice fragments. These deposits are widely distributed along river valleys and lowland areas. Overlying and interbedded with these sediments are volcanic deposits, including andesitic lava flows from Mount Marapi (Qama) and Mount Tandikat–Singgalang (Oast) [24].

Pleistocene volcanic products, represented by andesitic–basaltic pumice tuff (Qpt), are interpreted as deposits from the most recent eruptive phase of the Maninjau Caldera, particularly exposed in the western part of the caldera. In contrast, older metamorphic and sedimentary rocks of the Kuantan Formation (Permian–Carboniferous), consisting of phyllite, shale (PCks), and limestone (PCkl), crop out mainly in the northeastern sector near Lake Singkarak.

3.2. Identification of shallow fault structures

The inversion results indicate that four survey lines achieved RMS errors below 5%, suggesting a good fit between observed and calculated apparent resistivity data. The remaining three lines yielded RMS errors slightly above 5%, which is attributed to non-ideal field conditions such as poor electrode contact, dry or highly saturated soils, unstable electrode placement, and weather-related disturbances during data acquisition. Despite these limitations, the overall resistivity models remain interpretable and consistent with regional geological conditions.

The inverted resistivity sections exhibit distinct resistivity contrasts corresponding to different lithological units. High-resistivity zones are interpreted as compact volcanic rocks and massive limestone, whereas low-resistivity zones are associated with unconsolidated alluvial sediments, clay-rich volcanic tuffs, and fractured or weathered rock masses.

Electrical resistivity imaging surveys were conducted in Agam and Tanah Datar Regencies using a dipole–dipole electrode configuration, which provides enhanced sensitivity to lateral resistivity variations and is particularly effective for detecting near-vertical structures such as faults. The acquired datasets were processed using RES2DINV, and the resulting two-dimensional resistivity sections were analyzed to delineate subsurface lithology and identify fault-related features, taking into account the regional geological framework.

Table 2
Lithological information of the study area

Geological age	Formation / Unit	Lithology code	Lithological description
Quaternary (Holocene)	Surface deposits	Qal	Sand, silt, gravel, and reworked pumice tuff fragments
Quaternary (Holocene)	Volcanic rocks	Qama	Andesite from Mount Marapi
Quaternary (Holocene)	Volcanic rocks	Oast	Andesite from Mount Tandikat–Singgalang
Quaternary (Pleistocene)	Volcanic eruptive deposits	Qpt	Andesitic–basaltic pumice tuff from the latest eruption of the Maninjau Caldera
Permian–Carboniferous	Kuantan Formation	PCks	Phyllite and shale member
Permian–Carboniferous	Kuantan Formation	PCkl	Limestone member

Based on regional geological maps and previous studies (Table 2), the study area is composed of a wide range of lithological units, spanning from Quaternary to Permian–Carboniferous ages. The youngest units consist of Holocene alluvial deposits (Qal) composed of sand, silt, gravel, and reworked pumice fragments. These deposits are widely distributed along river valleys and lowland areas. Overlying and interbedded with these sediments are volcanic deposits, including andesitic lava flows from Mount Marapi (Qama) and Mount Tandikat–Singgalang (Oast).

3.3. Lithological characteristics and fault geometry derived from electrical resistivity profiles

Electrical resistivity imaging using the dipole–dipole configuration was conducted along seven survey lines (ATG, BPL, BKM, KBA, SWU,

BTP, and TGK) crossing the Sianok segment of the Sumatra Fault in Agam and Tanah Datar Regencies (Fig. 3). The survey lines generally trend northeast–southwest and intersect geomorphological lineaments associated with the fault zone. The resulting two-dimensional resistivity models provide insights into subsurface lithological variations and shallow fault geometries down to depths of approximately 20–53 m.

Across all profiles, subsurface resistivity values range from very low (<10 Ωm) to very high (>10^4 Ωm), reflecting variations in lithology, degree of weathering, and fluid content. Low-resistivity zones are commonly observed near the surface and are interpreted as clay-rich soils, weathered volcanic tuffs, or water-saturated sediments, particularly in cultivated alluvial plains and valley floors. In contrast, moderate resistivity values (≈20–100 Ωm) are associated with sandy layers and tuffaceous sandstones, while high resistivity anomalies (>300 Ωm) correspond to compact volcanic rocks, tuffaceous sandstones, and andesitic volcanic units, locally derived from Mount Marapi and the Tandikat–Singgalang volcanic complex.

Fault structures are consistently identified on the basis of lateral resistivity discontinuities, vertical to subvertical low-resistivity corridors, and offsets in resistivity layering. Along the ATG, BPL, BKM, KBA, SWU, and BTP profiles, these features indicate the presence of normal faults, characterized by downward displacement of lithological units on one side of the fault plane. The interpreted fault planes generally dip westward, consistent with the regional kinematic framework of the Sianok segment. These normal fault signatures are particularly well expressed within weathered volcanic and alluvial units, where fracturing and fluid infiltration significantly reduce bulk resistivity [20, 21, 25].

In contrast, the TGK profile exhibits a distinct resistivity pattern. Fault-related features along this line are marked by near-vertical resistivity discontinuities without significant vertical displacement of lithological layers, suggesting a strike-slip (horizontal) fault mechanism. This interpretation is consistent with the location of the TGK line within an intermontane valley near Lake Singkarak, where deformation is dominated by lateral shear rather than vertical offset.

Data quality assessment indicates that most profiles achieved low RMS inversion errors (<5%), confirming the reliability of the resistivity models. Profiles with higher RMS errors are attributed to non-ideal field conditions, including dry or highly saturated soils, unstable electrode placement, and cultural noise near roads or settlements. Despite these limitations, the overall structural patterns remain coherent and geologically consistent across the study area.

Overall, the integrated interpretation of all resistivity profiles reveals that the shallow subsurface along the Sianok segment is characterized by heterogeneous volcanic and sedimentary lithologies cut by multiple fault strands, dominated by normal faulting with localized strike-slip deformation. These results demonstrate the effectiveness of dipole–dipole electrical resistivity imaging in delineating shallow fault structures in complex volcanic–tectonic settings.

3.4. *Tectonic characteristics and their relationship with shallow fault structures*

The Sianok segment is part of the Sumatra Fault System and extends for approximately 90 km, characterized predominantly by dextral strike-slip motion parallel to the main fault trace. This strike-slip movement locally generates extensional zones within the crust, leading to subsidence in the central part of the fault zone and the formation of sag ponds. These sag ponds are typically associated with strike-slip faults and are observed near the BKM and BPL survey lines, aligned along a northwest–southeast direction consistent with the regional orientation of the Sumatra Fault [16, 26, 27].

A distinctive morphotectonic feature of the Sianok segment is the Sianok River Valley, which trends approximately 330°. Along this valley, the eastern block is relatively displaced southward, while the western block moves northward. In addition, several secondary lineaments develop along the valley, including erosional valleys trending 130°, which reflect dominant dextral strike-slip motion, and extensional valleys trending 90°, indicative of normal faulting. These geomorphic features suggest that deformation along the Sianok segment is not purely strike-slip, but involves localized extensional components.

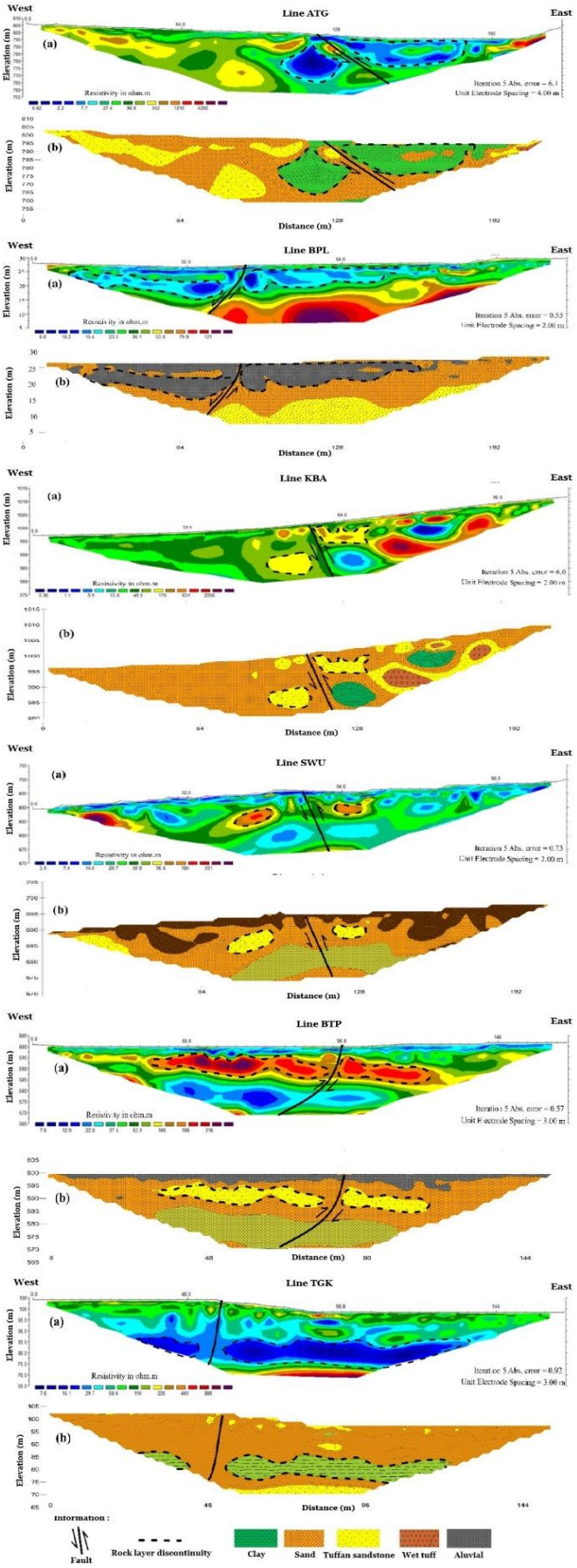

Fig. 3. Results of resistivity cross-section model interpretation on a 2D vertical cross-section.

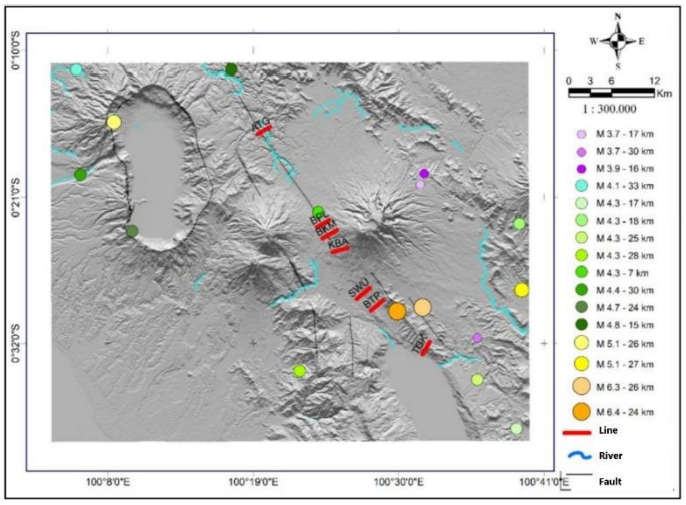

Fig. 4. Results of resistivity cross-section model interpretation on a 2D vertical cross-section.

The presence and activity of faults in the study area are further supported by high shallow seismicity. The seismicity map (Fig. 4) shows that earthquakes in the Agam and Tanah Datar regions are dominated by shallow events with focal depths less than 30 km, with hypocenters closely aligned with the Sumatra Fault lineament. This spatial relationship indicates that seismic activity in the study area is directly controlled by movements along the Sianok segment of the Sumatra Fault.

Historical records indicate at least 16 earthquake events within approximately 123 years in the study area. A significant event occurred in 2007, with magnitudes of 6.4 and 6.3, producing surface ruptures in the northern part of Lake Singkarak with a total length of about 22 km. These ruptures were also observed in the Batipuh area, where they cut across the main road and caused right-lateral displacement of approximately 5–12 cm, as well as severe damage to nearby buildings. Although the orientations of surface cracks vary locally, they are predominantly aligned in a northwest–southeast direction, consistent with the main trend of the Sumatra Fault [16].

Interpretation of the 2D electrical resistivity models indicates that the subsurface geology along the survey lines is dominated by sedimentary and volcaniclastic deposits, including clay, soil, alluvium, sand, sandstone, and tuffaceous sandstone. These units represent lahar-derived deposits composed mainly of tuff, andesite, and basaltic fragments. This interpretation is supported by the relatively low to moderate resistivity values (<400 Ωm) observed along the BPL, SWU, and BTP lines. Similar volcanic-derived deposits have been reported by Dahrin et al., who identified tuffaceous layers extending to depths of approximately 1 km within the Sianok Fault Zone.

Near-surface tuff deposits have undergone extensive weathering, particularly in cultivated areas such as rice fields, resulting in alluvial soils and soft clay layers characterized by relatively low resistivity values. Under dry conditions, however, these weathered layers may exhibit higher resistivity. The alluvial units commonly overlie more compact lahar deposits, such as sand, sandstone, and tuffaceous sandstone, which are expressed by higher resistivity contrasts in the resistivity sections.

From a mechanical perspective, rocks subjected to tectonic stress undergo deformation when the applied stress exceeds their elastic limit, resulting in faulting and displacement of rock layers. In this study, fault structures were identified based on resistivity discontinuities, vertical or subvertical low-resistivity zones, and offsets of resistivity layers in the 2D models. The interpreted fault planes were further constrained using regional geological maps, lithological resistivity references, and previous studies.

The resistivity models indicate the presence of fault structures along all survey lines. Along the ATG line, a fault is identified at distances of 116–120 m, with resistivity values ranging from 7.7 to 1,210 Ωm, separating clay and sand layers. This structure is interpreted as a normal fault with westward downthrow, consistent with lithological observations reported by [16]. Along the BPL line, a fault occurs at 40–44 m, with resistivity values of 25.4–53 Ωm, separating alluvial deposits and sand, and is also interpreted as a normal fault with westward displacement.

The BKM line reveals a fault at approximately 55 m, with resistivity values of 13.8–631 Ωm, separating tuffaceous sandstone and sand layers, and interpreted as a westward-dipping normal fault. Along the KBA line, a fault is identified at 145–150 m, characterized by high resistivity values (1,730–26,984 Ωm), separating wet tuff and sandstone, and interpreted as a normal fault with eastward downthrow.

Along the SWU line, two normal faults are identified at around 56 m, with resistivity values of 14–184 Ωm, separating tuffaceous sandstone and water-saturated sand layers, both exhibiting westward displacement. The BTP line shows a fault at 93–99 m, with resistivity values of 109–316 Ωm, separating tuffaceous sandstone units and interpreted as a normal fault with eastward downthrow.

In contrast, the TGK line exhibits a fault at 57–60 m, characterized by low resistivity values (7.6–15.1 Ωm) cutting through shale of the Kuantan Formation and infilled by sandstone. The fault plane is relatively steep and does not show significant vertical displacement of tuffaceous layers, suggesting a strike-slip fault mechanism. This interpretation is consistent with previous findings by Putra et al., who reported that the Sumatra Fault cuts phyllite and shale units of the Kuantan Formation as well as volcanic rocks in this area.

Geological structures can be identified using various approaches, including the analysis of satellite imagery such as Digital Elevation Models (DEMs), regional geological maps, geophysical data, and field observations of deformed rock outcrops exhibiting fault-related features. In this study, electrical resistivity data play a critical role in validating the presence of faults inferred from DEM-based lineament analysis, particularly linear valleys and ridge alignments, as shown in Fig. 5.

The Sianok Segment is clearly expressed in the DEM as a prominent linear valley associated with the main river course. From a geomorphological perspective, such linear valleys commonly represent mechanically weak zones within the crust and are frequently associated with fault structures. However, DEM analysis alone primarily indicates the surface expression and approximate location of faults, without providing detailed information on fault type, dip direction, or subsurface geometry, especially at shallow depths. To overcome these limitations, electrical resistivity surveys were conducted to characterize the shallow subsurface structure in greater detail. The processed resistivity data yielded two-dimensional resistivity models, which depict subsurface resistivity distributions through contour patterns, color contrasts, elevation, depth, and electrode spacing. Faults and lithological boundaries were interpreted based on resistivity discontinuities, abrupt lateral changes in resistivity values, and offsets in subsurface layering [28, 29].

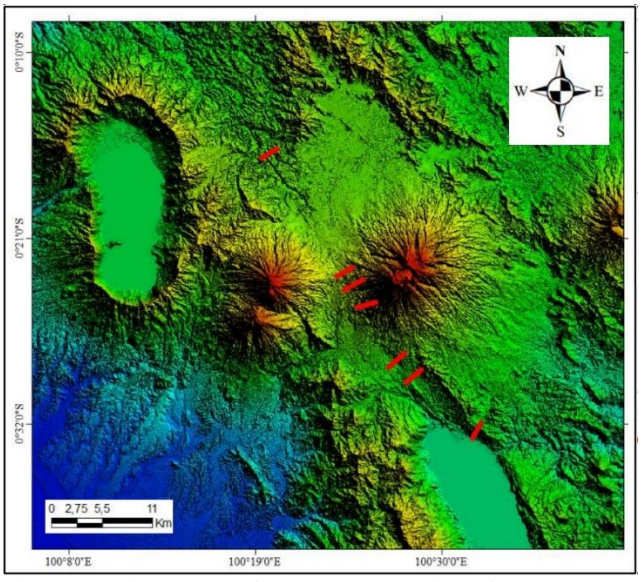

Fig. 5. DEM image map of Agam regency and Tanah Datar regency.

Interpretation of the seven resistivity profiles reveals the presence of fault structures along all survey lines. The identified fault types include a strike-slip fault on the TGK profile and normal faults on the remaining six profiles, characterized by downward displacement of rock layers. The normal faults generally exhibit westward-dipping geometries, indicating localized extensional deformation superimposed on the regional tectonic framework of the Sianok Segment. These results demonstrate a strong correlation between DEM-derived lineaments interpreted as part of the Sumatra Fault system and the subsurface fault structures delineated by electrical resistivity imaging. Consequently, the integration of geomorphological analysis using DEM data with electrical resistivity surveys proves to be an effective approach for identifying and validating shallow fault structures in tectonically active regions.

The integration of DEM-based lineament analysis with dipole–dipole electrical resistivity imaging to delineate the shallow structure of the Sianok Segment of the Sumatra Fault. This approach enables direct identification of fault geometry, dip direction, and fault type at shallow depths (<60 m), which cannot be resolved by geomorphological analysis alone. The results indicate that, despite its regional classification as a strike-slip fault, the shallow subsurface expression of the Sianok Segment is dominated by normal fault.

4. Conclusion

This study successfully delineates the presence and characteristics of shallow fault structures along the Sianok Segment of the Sumatra Fault using dipole–dipole Electrical Resistivity Imaging (ERI) integrated with DEM-based lineament analysis and regional geological data. The 2D resistivity inversion results reveal that fault zones are consistently detected across all survey lines, with resistivity values ranging from 7.6 to 29,684 Ωm, generally corresponding to unconsolidated to semi-consolidated materials such as sand and tuffaceous sandstone that occupy fault-related damage zones. The fault structures identified along the ATG, BPL, BKM, KBA, SWU, and BTP profiles are predominantly normal faults, characterized by downward displacement of lithological layers and fault planes dipping mainly toward the west. In contrast, the TGK profile exhibits a strike-slip fault geometry, indicated by a near-vertical fault plane without significant vertical displacement of the Kuantan Formation shale. This spatial variation in fault type highlights the structural complexity of the Sianok Segment, where the regional right-lateral motion of the Sumatra Fault is locally accompanied by extensional deformation.

The novelty of this study lies in the high-resolution delineation of shallow fault geometry through the integration of ERI-derived resistivity models and DEM-based geomorphological lineaments. Unlike previous studies that primarily relied on surface geomorphology or qualitative interpretations, this approach provides quantitative constraints on fault position, dip direction, fault type, and lithological characteristics within the shallow subsurface. These findings offer new insights into the near-surface expression of the Sianok Segment and contribute valuable information for seismic hazard assessment and risk mitigation in the Agam and Tanah Datar regions, West Sumatra, Indonesia.

CRediT authorship contribution statement

Gabriella A Sihite: Writing – review & editing, Writing – original draft, Supervision, Software, Resources, Methodology, Investigation, Formal analysis, Data curation. **Alamta Singarimbun:** Writing – review & editing, Supervision, Resources, Methodology, Investigation, Formal analysis, Data curation, Conceptualization. **Marjiyono:** Writing – review & editing, Investigation.

Declaration of Competing Interest

The authors declare that they have no known competing financial interests or personal relationships that could have appeared to influence the work reported in this paper.

Data availability

Data will be made available on request.

Acknowledgment

The authors gratefully acknowledge the Center for Geological Survey, Ministry of Energy and Mineral Resources of the Republic of Indonesia, for providing the electrical resistivity data used in this study. We also thank all parties who contributed to data processing, interpretation, and constructive discussions during the course of this research. The authors appreciate the use of Res2DInv, QGIS, Global Mapper, and Surfer software for data analysis and visualization. Constructive comments from reviewers are also acknowledged for improving the quality of this manuscript.

References

1. Hosono, T., Hartmann, J., Louvat, P., Amann, T., Washington, K. E., West, A. J., Okamura, K., Böttcher, M. E., and Gaillardet, J. (2018). Earthquake-Induced Structural Deformations Enhance Long-Term Solute Fluxes from Active Volcanic Systems, *Scientific Reports*, Vol. 8, No. 1, 1–12. doi:10.1038/s41598-018-32735-1.
2. Zhang, Z., Yao, H., Wang, W., and Liu, C. (2021). 3-D Crustal Azimuthal Anisotropy Reveals Multi-Stage Deformation Processes of the Sichuan Basin and Its Adjacent Journal of Geophysical Research : Solid Earth, *Journal of Geophysical Research: Solid Earth*, Vol. 127, No. e2021JB023289, 1–17. doi:10.1029/2021JB023289.
3. Liu, S., Suardi, I., Xu, X., Yang, S., and Tong, P. (2021). The Geometry of the Subducted Slab Beneath Sumatra Revealed by Regional and Teleseismic Traveltime Tomography, *Journal of Geophysical Research: Solid Earth*, Vol. 126, No. 1, 1–29. doi:10.1029/2020JB020169.
4. Dewi, K. C. S., Siregar, R. N., Ningati, T. I., Pulungan, Z. N., Indriyawati, A., and Takahashi, H. (2025). Analysis of Subsurface Faults Using 3D Gravity Method Based On Satellite Image Data : Insights into Indo-Australian and Eurasian Plate Subduction in the Formation of An Accretionary Prism, *International Journal of Hydrological and Environmental for Sustainability*, Vol. 4, No. 3, 135–148.
5. Hariyono, E., and S, L. (2018). The Characteristics of Volcanic Eruption in Indonesia, *Volcanoes - Geological and Geophysical Setting, Theoretical Aspects and Numerical Modeling, Applications to Industry and Their Impact on the Human Health*, No. July. doi:10.5772/intechopen.71449.
6. McCaffrey, R. (2009). The Tectonic Framework of the Sumatran Subduction Zone, *Annual Review of Earth and Planetary Sciences*, Vol. 37, 345–366. doi:10.1146/annurev.earth.031208.100212.
7. Hristov, V., Stoyanov, N., Valtchev, S., Kolev, S., and Benderev, A. (2019). Utilization of Low Enthalpy Geothermal Energy in Bulgaria, *IOP Conference Series: Earth and Environmental Science*, Vol. 249, No. 1. doi:10.1088/1755-1315/249/1/012035.
8. Taruna, R. M., and Banyunegoro, V. H. (2018). Earthquake Relocation Using Double Difference Method for 2D Modelling of Subducting Slab and Back Arc Thrust in West Nusa Tenggara, *Jurnal Penelitian Fisika Dan Aplikasinya (JPFA)*, Vol. 8, No. 2, 132. doi:10.26740/jpfa.v8n2.p132-143.
9. Collings, R., Lange, D., Rietbrock, A., Tilmann, F., Natawidjaja, D., Suwargadi, B., Miller, M., and Saul, J. (2012). Structure and Seismogenic Properties of the Mentawai Segment of the Sumatra Subduction Zone Revealed by Local Earthquake Traveltime Tomography, *Journal of Geophysical Research*, Vol. 117, 1–23. doi:10.1029/2011JB008469.
10. Jihad, A., Muksin, U., Syamsidik, and Ramli, M. (2021). Earthquake Relocation to Understand the Megathrust Segments along the Sumatran Subduction Zone, *IOP Conference Series: Earth and Environmental Science*, Vol. 630, 012002. doi:10.1088/1755-1315/630/1/012002.
11. Xu, J., and Kono, Y. (2002). Geometry of Slab, Intraslab Stress Field and Its Tectonic Implication in the Nankai Trough, Japan, *Earth, Planets and Space*, Vol. 54, No. 7, 733–742. doi:10.1186/BF03351726.
12. Kusuhara, F., Kazahaya, K., Morikawa, N., Yasuhara, M., Tanaka, H., Takahashi, M., and Tosaki, Y. (2020). Original Composition and Formation Process of Slab-Derived Deep Brine from Kashio Mineral Spring in Central Japan, *Earth, Planets and Space*, Vol. 72, No. 1. doi:10.1186/s40623-020-01225-y.

13. Malod, J. A., Karta, K., Beslier, M. O., and Zen, M. T. (1995). From Normal to Oblique Subduction: Tectonic Relationships between Java and Sumatra, *Journal of Southeast Asian Earth Sciences*, Vol. 12, Nos. 1–2, 85–93. doi:10.1016/0743-9547(95)00023-2.

14. Li, C. F. (2011). An Integrated Geodynamic Model of the Nankai Subduction Zone and Neighboring Regions from Geophysical Inversion and Modeling, *Journal of Geodynamics*, Vol. 51, No. 1, 64–80. doi:10.1016/j.jog.2010.08.003.

15. Stern, R. J. (2002). Subduction Zones, *Reviews of Geophysics*, Vol. 40, No. 4, 3-1-3–38. doi:10.1029/2001RG000108.

16. Utama, H. W., Mulyasari, R., and Said, Y. M. (2021). Geothermal Potential on Sumatra Fault System To Sustainable Geotourism in West Sumatra, *JGE (Jurnal Geofisika Eksplorasi)*, Vol. 7, No. 2, 126–137. doi:10.23960/jge.v7i2.128.

17. Tabei, T., Hashimoto, M., Miyazaki, S., Hirahara, K., Kimata, F., Matsushima, T., Tanaka, T., Eguchi, Y., Takaya, T., Hoso, Y., Ohya, F., and Kato, T. (2002). Subsurface Structure and Faulting of the Median Tectonic Line, Southwest Japan Inferred from GPS Velocity Field, *Earth, Planets and Space*, Vol. 54, No. 11, 1065–1070. doi:10.1186/BF03353303.

18. Tongkul, F. (2017). Active Tectonics in Sabah – Seismicity and Active Faults, *Bulletin of the Geological Society of Malaysia*, Vol. 64, No. December, 27–36. doi:10.7186/bgsm64201703.

19. Maryanto, S. (2017). Geo Techno Park Potential at Arjuno-Welirang Volcano Hosted Geothermal Area, Batu, East Java, Indonesia (Multi Geophysical Approach), *AIP Conference Proceedings*, Vol. 1908, No. 2017. doi:10.1063/1.5012712.

20. Sujitapan, C., Kendall, J. M., Chambers, J. E., and Yordkayhun, S. (2024). Landslide Assessment through Integrated Geoelectrical and Seismic Methods: A Case Study in Thungsong Site, Southern Thailand, *Heliyon*, Vol. 10, No. 2. doi:10.1016/j.heliyon.2024.e24660.

21. Chambers, J., Holmes, J., Whiteley, J., Boyd, J., Meldrum, P., Wilkinson, P., Kuras, O., Swift, R., Harrison, H., Glendinning, S., Stirling, R., Huntley, D., Slater, N., and Donohue, S. (2022). Long-Term Geoelectrical Monitoring of Landslides in Natural and Engineered Slopes, *Leading Edge*, Vol. 41, No. 11, 768–767. doi:10.1190/tle41110768.1.

22. Whiteley, J. S., Watlet, A., Uhlemann, S., Wilkinson, P., Boyd, J. P., Jordan, C., Kendall, J. M., and Chambers, J. E. (2021). Rapid Characterisation of Landslide Heterogeneity Using Unsupervised Classification of Electrical Resistivity and Seismic Refraction Surveys, *Engineering Geology*, Vol. 290, No. May, 106189. doi:10.1016/j.enggeo.2021.106189.

23. Martinho, E. (2023). *Electrical Resistivity and Induced Polarization Methods for Environmental Investigations: An Overview*, *Water, Air, and Soil Pollution* (Vol. 234), Springer International Publishing. doi:10.1007/s11270-023-06214-x.

24. Kusumayudha, S. B., Lestari, P., and Paripurno, E. T. (2018). Eruption Characteristic of the Sleeping Volcano, Sinabung, North Sumatera, Indonesia, and SMS Gateway for Disaster Early Warning System, *Indonesian Journal of Geography*, Vol. 50, No. 1, 70–77. doi:10.22146/ijg.17574.

25. Meju, M. A., and Le, L. (2002). Geoelectromagneticexploration For Natural Resources:Models, Case Studies and Challenges, *Surveys in Geophysics*, Vol. 23, 133–205.

26. Lange, D., Tilmann, F., Henstock, T., Rietbrock, A., Natawidjaja, D., and Kopp, H. (2018). Structure of the Central Sumatran Subduction Zone Revealed by Local Earthquake Travel-Time Tomography Using an Amphibious Network, *Solid Earth*, Vol. 9, No. 4, 1035–1049. doi:10.5194/se-9-1035-2018.

27. Lin, J. Y., Sibuet, J. C., Hsu, S. K., and Wu, W. N. (2014). Could a Sumatra-like Megathrust Earthquake Occur in the South Ryukyu Subduction Zone?, *Earth, Planets and Space*, Vol. 66, No. 1, 1–8. doi:10.1186/1880-5981-66-49.

28. Siringoringo, L. P., Sapiie, B., Rudyawan, A., and Sucipta, I. G. B. E. (2024). Origin of High Heat Flow in the Back-Arc Basins of Sumatra: An Opportunity for Geothermal Energy Development, *Energy Geoscience*, Vol. 5, No. 3, 100289. doi:10.1016/j.engeos.2024.100289.

29. Hochstein, M. P., and Sudarman, S. (1993). Geothermal Resources of Sumatra, *Geothermics*, Vol. 22, No. 3, 181–200. doi:10.1016/0375-6505(93)90042-L.